Gravity waves generated by sheared potential-vorticity anomalies

François Lott[†], Riwal Plougonven[†] and Jacques Vanneste[‡]

[†]Laboratoire de Météorologie Dynamique du CNRS

Ecole Normale Supérieure, 24, rue Lhomond, 75231 Paris cedex 05, France

[‡]School of Mathematics and Maxwell Institute for Mathematical Sciences

University of Edinburgh, Edinburgh EH9 3JZ, UK

March 6, 2009

Abstract

The gravity waves generated by potential-vorticity anomalies in a rotating stratified shear flow are examined under the assumptions of constant vertical shear, two-dimensionality and unbounded domain. Near a potential-vorticity anomaly, the associated perturbation is well modelled by quasi-geostrophic theory. This is not the case at large vertical distances, however, and in particular beyond the two inertial layers that appear above and below the anomaly; there, the perturbation is made of vertically propagating gravity waves. This structure is described analytically, using an expansion in the continuous spectrum of the singular modes that results from the presence of critical levels.

Several explicit results are obtained. These include the form of the Eliassen–Palm flux as a function of the Richardson number N^2/Λ^2, where N is the Brunt–Väisälä frequency and Λ the vertical shear. Its non-dimensional value is shown to be approximately $\exp(-\pi N/\Lambda)/8$ in the far-field, gravity-wave region, and approximately twice that between the two inertial layers. These results, which imply substantial wave-flow interactions in the inertial layers, are valid for Richardson numbers larger than 1, and for a large range of potential-vorticity distributions; In dimensional form they provide simple relationships between the Eliassen–Palm fluxes and the large-scale flow characteristics.

As an illustration, we consider a potential-vorticity disturbance with an amplitude of 1 PVU and a depth of 1 km, and estimate that the associated Eliassen–Palm flux ranges between 0.1 mPa and 100 mPa for a Richardson number between 1 and 10. These values of the flux compare with those observed in the lower stratosphere, which suggests that the mechanism identified in this paper provides a substantial gravity-wave source, one that could be parameterized in GCMs.

1 Introduction

It is well established that gravity waves (GWs) have a substantial influence on the large-scale atmospheric circulation, particularly in the middle atmosphere. As a result, sources of atmospheric GWs have received a great deal of attention. Significant tropospheric sources include topography, convective and frontal activities (Bretherton and Smolarkiewicz 1989; Shutts and Gray 1994), wind-shear instabilities (Lalas and Einaudi 1976, Rosenthal and Lindzen 1983,

Lott et al. 1992), nonmodal growth (Lott 1997, Bakas and Ioannou 2007) and geostrophic adjustment.

When it comes to geostrophic adjustment, one should distinguish classical adjustment, in which an initially unbalanced flow radiates GWs as it returns to near-geostrophic balance (Rossby 1937, Blumen 1972, Fritts and Luo 1992), from spontaneous adjustment, in which a well-balanced flow radiates weakly GWs in the course of its (near-balanced) evolution (Ford et al. 2000). The source of GW activity differs between the two types of adjustment. In the first case, GW generation should be attributed to the mechanism responsible for the initial imbalance rather than to the adjustment.[1] In the second case, spontaneous adjustment itself is the GW source.

Spontaneous adjustment, on which the present paper focuses, has been the subject of intense research activity. Much of this has been motivated by theoretical issues related to the limitations of balanced models and the non-existence of exactly invariant slow manifolds (e.g., Vanneste 2008 and references therein). There are however practical implications, in particular for the parameterization of non-orographic GWs in general circulation models, since the (pseudo)momentum flux associated with the GWs generated spontaneously may well be significant. To assess this, it is important to quantify the GW activity generated by simple, physically plausible processes. This is the main aim of this paper.

The process we examine is the generation of GWs that results from the advection of potential-vorticity (PV) anomalies by a vertically sheared wind. Since we consider background flow with uniform PV, it is related to the work of Plougonven et al (2005) on the unbalanced instabilities associated with surface edge waves (see also Molemaker et al 2005). In our case, however, there is no boundary, and the PV disturbance is imposed within the flow and can have a finite vertical extent. The process we examine is also related to the work of Vanneste and Yavneh (2004) and Olafsdottir et al (2008) on GWs generated by PV anomalies in a horizontal shear with the difference that the wind shear is vertical in our case. A common feature of all these processes, one which is likely generic for spontaneous-generation phenomena (Vanneste 2008), is that the GW-activity is exponentially weak in the limit of small Rossby number, or equivalently large Richardson number. Our study, which is not restricted to this limit, confirms this conclusion; it nevertheless suggests that for reasonable values of the parameters, the GW amplitudes generated by PV anomalies in a vertical shear can be significant, comparable for instance with those observed in the low stratosphere by constant level balloons far from mountain ranges (Hertzog et al. 2008).

In the background flow that we consider, with uniform-PV, the small-amplitude PV anomalies are advected passively by the shear. The spectral representation of this dynamics involves a continuous spectrum of singular modes whose phase velocity is in the range of the basic-flow velocity, $(-\infty, \infty)$ in the unbounded domain that we assume. The vertical structure of the PV associated with the singular modes is simple: each mode is represented by a Dirac distribution centred at the critical level, where the phase velocity equals the basic flow velocity (see Pedlosky 1979 for a discussion of the analogous continuous spectrum in the quasi-geostrophic Eady problem). The fields decay rapidly above and below the critical level as far as the inertial levels where the Doppler-shifted frequency is equal to the Coriolis parameter (Jones 1967). Beyond these levels, the structure is oscillatory and can be identified as the GW-signature of the (Dirac) PV anomaly.

The first purpose of this paper is to obtain the vertical structure of the singular modes with Dirac PV analytically. The second is to deduce, by integration over the continuous spectrum,

[1] It is in this context that Scavuzzo et al. (1998) and Lott (2003) attributed the presence of inertia-gravity waves near mountains to a large-scale adjustment to breaking small-scale gravity waves.

the GW response to a vertically smooth, localised PV distribution. The third is to show that this GW response can yield substantial Eliassen–Palm (or pseudomomentum) fluxes at large vertical distances from the PV anomaly. Interestingly, we find that about half (exactly so in the limit of large Richardson number) of the pseudomomentum generated by the advection of PV is transported by GWs over arbitrarily large distances; the other half is deposited in an inertial-levels region, where substantial wave–flow interactions likely take place.

The plan of the paper is as follows. The general formulation of the problem, and its transformation to a dimensionless form are given in the Section 2. Section 3 is devoted to the derivation of the vertical structure of the singular modes associated with a Dirac in PV. In Section 4 we rephrase the result of Section 3 in dimensional terms and estimate the amplitude of the pseudomomentum fluxes that can be expected from horizontally monochromatic PV anomalies; these compare with those measured in the lower stratosphere during field campaigns. We also consider PV distributions that are localised horizontally and have a finite-depth, so that the GW response is transient. In Section 5, we summarize our results and discuss their significance for (i) the parameterization of GWs in GCMs, (ii) the transient evolution of baroclinic disturbances, and (iii) the treatment of the more general initial-value problem. An appendix is devoted to approximate solutions valid in the limit of large Richardson number.

2 General formulation

2.1 Disturbance equations and potential vorticity

In the absence of mechanical and diabatic forcings, the hydrostatic–Boussinesq equations for the evolution of a two-dimensional disturbance in the uniformly sheared flow $\overline{\mathbf{u}}_{\mathbf{0}} = (\Lambda z, 0, 0)$, where $\Lambda > 0$ denotes the shear, read

$$(\partial_t + \Lambda z \partial_x)\, u' + \Lambda w' - f v' = -\frac{1}{\rho_r}\partial_x p', \tag{2.1a}$$

$$(\partial_t + \Lambda z \partial_x)\, v' + f u' = 0, \tag{2.1b}$$

$$0 = -\frac{1}{\rho_r}\partial_z p' + g\frac{\theta'}{\theta_r}, \tag{2.1c}$$

$$(\partial_t + \Lambda z \partial_x)\, g\frac{\theta'}{\theta_r} - f\Lambda v' + N^2 w' = 0, \tag{2.1d}$$

$$\partial_x u' + \partial_z w' = 0. \tag{2.1e}$$

Here u', v', and w' are the three components of the velocity disturbance, p' is the pressure disturbance, ρ_r is a constant reference density, θ' is the potential temperature disturbance, θ_r is a constant reference potential temperature, g is the gravity constant, f is the Coriolis parameter, and $N^2 = g\overline{\theta}_{0z}/\theta_r$ is the square of the constant Brunt–Väisälä frequency, with $\overline{\theta}_0(y, z)$ the background potential-temperature. Note that Λ appears in (2.1d) because the background shear flow is in thermal wind balance, $\overline{\theta}_{0y} = -\theta_r f\Lambda/g$.

Equations (2.1a)–(2.1e) imply the conservation equation

$$(\partial_t + \Lambda z \partial_x)\, q' = 0, \tag{2.2}$$

for the potential-vorticity (PV) perturbation

$$q' = \frac{1}{\rho_r}\left(\overline{\theta}_{0z}\partial_x v' + \overline{\theta}_{0y}\partial_z u' + f\partial_z\theta'\right). \tag{2.3}$$

It follows that the PV at any time t is given explicitly in terms of the initial condition $q'_0(x,z) = q'(x,z,t=0)$ by

$$q'(x,z,t) = q'_0(x - \Lambda z t, z). \tag{2.4}$$

2.2 Normal-mode decomposition

To evaluate the disturbance field associated with the PV anomaly (2.4), we express this solution in Fourier space,

$$q'(x,z,t) = \int_{-\infty}^{+\infty} \hat{q}(k,z,t) e^{ikx} dk = \int_{-\infty}^{+\infty} \hat{q}_0(k,z) e^{i(kx - \Lambda z t)} dk, \tag{2.5}$$

where $\hat{q}_0$ is the Fourier transform of q'_0, satisfying

$$q'_0(k,z) = \int_{-\infty}^{\infty} \hat{q}_0(k,z) e^{+ikx} dk. \tag{2.6}$$

We rewrite (2.5) in the form

$$q'(x,z,t) = \int_{-\infty}^{+\infty} \int_{-\infty}^{+\infty} \hat{q}_0(k,z') e^{ik(x - \Lambda z' t)} \frac{k\Lambda}{f} \delta\left(\frac{k\Lambda}{f}(z - z')\right) dz' dk, \tag{2.7}$$

where $\delta(\xi)$ is the Dirac function of the variable

$$\xi = \frac{k\Lambda}{f}(z - z'). \tag{2.8}$$

Note that (2.7) can be interpreted as the expansion of the perturbation PV in the (singular) normal modes of (2.3); these modes form a continuum, parameterised by the phase speed $\Lambda z'$. The scaling used in (2.8) places the inertial levels of these modes at $\xi = \pm 1$ (Inverarity and Shutts 2000).

We are interested in the response of other fields, which can display GW activity, to the evolving PV (2.5). As a representative of these fields, we mainly focus on the perturbation streamfunction ψ', related to the perturbation velocity in the (x,z)-plane according to

$$u' = \partial_z \psi' \quad \text{and} \quad w' = -\partial_x \psi'. \tag{2.9}$$

The expansion of the streamfunction corresponding to the expansion (2.7) of the PV can be written as

$$\psi' = \int_{-\infty}^{+\infty} \int_{-\infty}^{+\infty} \hat{\psi}_0(k,z') e^{ik(x - \Lambda z' t)} \Psi\left(\frac{k\Lambda}{f}(z - z')\right) dz' dk, \tag{2.10}$$

where $\hat{\psi}_0(k,z')$ is the amplitude of the normal mode, and $\Psi(\xi)$ its vertical structure. Note that this expansion, which describes the part of ψ' slaved to the PV, is not complete: an additional continuum of singular modes, representing free sheared GWs, would need to be added to the expansion to solve an arbitrary initial-value problem.

The velocities u', v', w' and the potential temperature θ' have expansions analogous to (2.10), with $\hat{\psi}_0$ replaced by $\hat{u}_0$, $\hat{v}_0$, $\hat{w}_0$ and $\hat{\theta}_0$, and Ψ replaced by U, V, W. Introducing these expansions into (2.1a)–(2.1e), and choosing

$$\hat{u}_0 = \frac{k\Lambda}{f}\hat{\psi}_0, \;\; \hat{v}_0 = i\frac{k\Lambda}{f}\hat{\psi}_0, \;\; \hat{w}_0 = -ik\hat{\psi}_0, \;\; \text{and } \hat{\theta}_0 = \frac{\theta_r k \Lambda^2}{fg}\hat{\psi}_0 \tag{2.11}$$

gives

$$U = \Psi_\xi,\ V = \frac{\Psi_\xi}{\xi},\ W = \Psi \text{ and } \Theta = \frac{\Psi_\xi}{\xi^2} + \frac{J\Psi}{\xi}, \tag{2.12}$$

where we have introduced the Richardson number

$$J = N^2/\Lambda^2. \tag{2.13}$$

We now introduce (2.11)–(2.12), into the expressions (2.3) and (2.7) for the PV. Choosing the streamfunction amplitude

$$\hat{\psi}_0(k, z') = \frac{g}{k\theta_r \Lambda^2} \rho_r \hat{q}_0(k, z'), \tag{2.14}$$

then leads to the differential equation

$$\left(\frac{1-\xi^2}{\xi^2}\right)\Psi_{\xi\xi} - \frac{2}{\xi^3}\Psi_\xi - \frac{J}{\xi^2}\Psi = \delta(\xi), \tag{2.15}$$

for the streamfunction structure $\Psi(\xi)$. We solve this equation explicitly in the next section.

3 Evaluation of $\Psi(\xi)$

To find a solution to (2.15), we first derive its homogeneous solutions for $\xi > 0$, and impose a radiation condition for $\xi \gg 1$ to obtain a solution which represents an upward-propagating GW. We deduce from this a solution valid for $\xi < 0$ which represents a downward-propagating GW for $\xi \ll -1$. The amplitudes of these two solutions are then chosen to satisfy the jump condition associated with (2.15), that is,

$$\left[\frac{\Psi_\xi}{\xi^2}\right]_{0^-}^{0^+} = 1. \tag{3.1}$$

3.1 Homogeneous solution for $\xi > 0$

The change of variable $\eta = \xi^2$ transforms (2.15) into the canonical form of the hypergeometric equation (Eq. 15.5.1 in Abramowitz and Stegun 1964, hereafter AS):

$$\eta\,(1-\eta)\,\Psi_{\eta\eta} + (c - (a+b+1)\,\eta)\Psi_\eta - ab\,\Psi = 0, \tag{3.2a}$$

$$\text{where} \quad a = -\frac{1}{4} + \frac{i}{2}\mu,\ b = a^*,\ c = -\frac{1}{2} = a + b \text{ and } \mu = \sqrt{J - 1/4}. \tag{3.2b}$$

Note that $a + b - c = 0$, a relation that is related to the fact that the two inertial levels at $\xi = \pm 1$ are logarithmic singularities of (2.15), as described by Jones (1967).

For $\xi > 1$ we retain one of the two independent solutions of the hypergeometric equations (see AS, 15.5.8), written as

$$\Psi^{(u)}(\xi) = \xi^{-2b} F\left(a', b'; a' + b'; \xi^{-2}\right), \tag{3.3}$$

where F denotes the hypergeometric function, and $a' = a^*$ and $b' = 1 - a$. We retain this solution because its asymptotic form,

$$\Psi^{(u)}(\xi) \sim \xi^{1/2 + i\mu} \quad \text{as } \xi \to \infty, \tag{3.4}$$

corresponds to a GW propagating upward (Booker and Bretherton, 1967). The other solution (given by 15.5.7 in AS) corresponds to a GW propagating downward.

For $0 < \xi < 1$ the solution to (3.2a) is best written as a linear combination of the two independent solutions

$$\Psi^{(u)}(\xi) = A\, F(a, b; a+b; \xi^2) \;+\; B\, \xi^3\, F(a'', b''; a''+b''; \xi^2) \tag{3.5}$$

where $a'' = 1 - a^*$, $b'' = 1 - a$, and A and B are two complex constants (15.5.3–4 in AS). To connect this solution to (3.3), we use a transformation formula for F (15.3.10 in AS) and obtain the asymptotic approximations

$$\Psi^{(u)}(\xi) \sim \alpha' \ln(\xi - 1) + \beta' \quad \text{as } \xi \to 1^+, \tag{3.6a}$$

$$\Psi^{(u)}(\xi) \sim (\alpha A + \alpha'' B) \ln(1 - \xi) + \beta A + \beta'' B \quad \text{as } \xi \to 1^-. \tag{3.6b}$$

In these expressions,

$$\alpha = -\frac{\Gamma(a+b)}{\Gamma(a)\Gamma(b)} \quad \text{and} \quad \beta = \alpha\left[\psi_d(a) + \psi_d(b) + \ln(2) - 2\psi_d(1)\right], \tag{3.7}$$

where Γ is the gamma function and ψ_d is the digamma function (see AS, chapter 6). The other coefficients (α', β') and (α'', β'') are defined by the same formulas with (a, b) replaced by (a', b') and (a'', b'') respectively.

To continue the solution (3.6a) below the inertial level at $\xi = 1$, we follow Booker and Bretherton (1967) and introduce a infinitely small linear damping which shifts the real ξ-axis into the lower half of the complex plane so that

$$\xi - 1 = (1 - \xi) e^{-i\pi} \quad \text{for} \quad \xi < 1. \tag{3.8}$$

Thus, (3.6a) matches (3.6b) provided that

$$\alpha A + \alpha'' B = \alpha' \quad \text{and} \quad \beta A + \beta'' B = \beta' - i\pi\alpha'. \tag{3.9}$$

Solving for A and B gives

$$A = \frac{\sqrt{\pi}}{2} \frac{\Gamma(1 - i\mu)}{\Gamma(\frac{5}{4} - i\frac{\mu}{2})^2} e^{+i\pi a^*} \quad \text{and} \quad B = -\frac{4\sqrt{\pi}}{3} \frac{\Gamma(1 - i\mu)}{\Gamma(-\frac{1}{4} - i\frac{\mu}{2})^2} e^{-i\pi a}, \tag{3.10}$$

after simplifications using reflection formulas for the gamma and digamma functions (6.1.17 and 6.3.7 in AS). This completes the determination of $\Psi^{(u)}(\xi)$.

3.2 Solution over the entire domain

The solution for $\xi < 0$ can be deduced from $\Psi^{(u)}(\xi)$ by noting that (2.15) only contains real coefficients and is even. A possible solution is simply

$$\Psi^{(d)}(\xi) = \Psi^{(u)}(-\xi)^*. \tag{3.11}$$

This satisfies the radiation condition for $\xi \to -\infty$ since

$$\Psi^{(d)}(\xi) \sim (-\xi)^{1/2 - i\mu}, \tag{3.12}$$

which represents a downward-propagating GW.

The two solutions $\Psi^{(u)}$ and $\Psi^{(d)}$ can be combined to obtain a solution valid over the entire domain which satisfies the jump condition (3.1). This is given by

$$\Psi(\xi) = \begin{cases} \dfrac{A^*\Psi^{(u)}(\xi)}{3(BA^* + AB^*)} & \text{for } \xi > 0 \\ \dfrac{A\Psi^{(d)}(\xi)}{3(BA^* + AB^*)} & \text{for } \xi < 0 \end{cases}. \tag{3.13}$$

The jump condition is readily verified by noting that if $|\xi| < 1$,

$$\Psi(\xi) = \frac{A^*A}{BA^* + A^*B} F(a, b; a + b; \xi^2) + \frac{BA^*\xi^3}{3(BA^* + AB^*)} F(a'', b''; a'' + b''; \xi^2) \text{ for } \xi > 0, \tag{3.14a}$$

$$\Psi(\xi) = \frac{A^*A}{BA^* + A^*B} F(a, b; a + b; \xi^2) - \frac{AB^*\xi^3}{3(BA^* + AB^*)} F(a'', b''; a'' + b''; \xi^2) \text{ for } \xi < 0. \tag{3.14b}$$

The first terms on the right-hand sides of (3.14a)–(3.14b) are identical and hence do not contribute to the jump (3.1); the second terms combine so that Ψ_ξ/ξ^2 jumps by 1 at $\xi = 0$ as required.

Several conclusions can be derived from the explicit form (3.13) of the streamfunction $\Psi(\xi)$. First, for small $|\xi|$, $\Psi(\xi)$ approaches the value

$$\Psi(0) = \frac{AA^*}{3(AB^* + A^*B)} \overset{J\gg 1}{\sim} \frac{1}{2J^{3/2}}, \tag{3.15}$$

where the symbol $\overset{J\gg 1}{\sim}$ is used to denote the asymptotic behaviour for large J. This asymptotic estimate, derived here using Stirling's formula for the gamma function (see AS 6.1.37), is also obtained when the quasi-geostrophic approximation of (2.15) is solved (see Appendix A.1). Second, we obtain from (3.4) and (3.13) that

$$\Psi \sim E\xi^{1/2+i\mu} \text{ as } \xi \to \infty, \tag{3.16}$$

where

$$E = \frac{A^*}{3(AB^* + A^*B)} = -A^*\frac{e^{-\pi\mu}}{2\mu}. \tag{3.17}$$

The behaviour as $\xi \to -\infty$ is similar. Accordingly, the amplitude of the GWs in the far-field $|\xi| \gg 1$ is

$$|E| = \frac{|\Gamma(1 + i\mu)|}{|\Gamma(\frac{5}{4} + i\frac{\mu}{2})|}\frac{\sqrt{\pi}}{2}\frac{e^{-\pi\mu/2}}{\mu} \overset{J\gg 1}{\sim} \frac{e^{-\pi\sqrt{J}/2}}{2J}. \tag{3.18}$$

The large-J approximation in (3.18) is one of the main results of this paper. Obviously it cannot be recovered in the quasi-geostrophic approximation, which filters out GWs completely, but it can be recovered by a WKB treatment of (2.15). This is demonstrated in Appendix A.2.

A third result derived from (3.13) concerns the EP flux (Eliassen and Palm 1961), or pseudomomentum flux, associated with the solution $\Psi(\xi)$. Multiplying (2.15) by $J^{3/2}\Psi^*$ and integrating by parts results in a conservation relation for the non-dimensional EP flux

$$\mathcal{F}^\xi = \text{Re}\left(\frac{iJ^{3/2}}{2}\frac{1 - \xi^2}{\xi^2}\Psi_\xi\Psi^*\right) = \text{const.}, \tag{3.19}$$

that is valid away from $\xi = 0, \pm 1$. Using the asymptotic approximation (3.16) shows that $\mathcal{F}^\xi = \mu J^{3/2}|E|^2/2$ for $|\xi| > 1$. The flux $\mathcal{F}^\xi$ is discontinuous across the inertial level $\xi = 1$.

To evaluate its jump, we use the approximations (3.6a)–(3.7) valid for $\xi \to 1^{\pm}$ to find that $\mathcal{F}^{\xi}(1^+) - \mathcal{F}^{\xi}(1^-) = -\pi J^{3/2}|E|^2|\alpha''|^2$. Finally, the Taylor series expansions of (3.14a)–(3.14b) near $\xi = 0$ shows that the flux is continuous across $\xi = 0$: $\mathcal{F}^{\xi}(0^+) - \mathcal{F}^{\xi}(0^-) = 0$. Using the explicit expression of α'' and Stirling's formula, our results for the EP flux are summarized as follows:

$$\mathcal{F}^{\xi} = \begin{cases} \dfrac{\mu}{2} J^{3/2}|E|^2 \overset{J\gg 1}{\sim} \dfrac{e^{-\pi\sqrt{J}}}{8} & \text{for } |\xi| > 1 \\ (1+\coth(\mu\pi))\,\dfrac{\mu}{2} J^{3}|E|^2 \overset{J\gg 1}{\sim} \dfrac{e^{-\pi\sqrt{J}}}{4} & \text{for } |\xi| < 1 \end{cases} . \tag{3.20}$$

This shows, in particular, that the GWs produced by the PV anomalies deposit almost as much momentum at the inertial levels as they transport in the far-field.

3.3 Results

The four panels in Fig. 1 show the solution (3.13) for Ψ for four values of the Richardson number J. For all values of J, the streamfunction amplitude decays away from $\xi = 0$ in the region between $\xi = \pm 1$, where it has an almost constant phase, indicating a non-propagating character. The decay for small ξ is well predicted by the quasi-geostrophic approximation Ψ_g, also shown, which behaves essentially like $\exp(-\sqrt{J}|\xi|)$ (see Appendix A.1).

Beyond the inertial levels, that is for $|\xi| > 1$, the disturbance is propagating, with the real and imaginary part of Ψ in quadrature. The asymptotic behaviour $E\xi^{1/2+i\mu}$ as $|\xi| \to \infty$ is also shown in Fig. 1: it corresponds to a pure GW in our context. The amplitude $|E|$ of the far-field GW, given in (3.18), is compared in Fig. 2 with its large-J asymptotic estimate, also given in (3.18). The figure confirms the validity of this estimate and shows that it remains useful for values of J as small as 1. The figure also highlights the rapid decrease of the GW amplitude with J that is encapsulated in the exponential factor $\exp(-\sqrt{J}\pi/2)$ appearing in the asymptotic estimate. A crude argument is suggestive of this dependence: if the quasi-geostrophic approximation is used (well beyond its range of validity) up to the inertial levels $\xi = \pm 1$, the amplitude attained there, and hence the GW amplitude, is predicted to be roughly $\exp(-\sqrt{J})$. The presence of the factor $\pi/2$ can be traced to the breakdown of the quasi-geostrophic approximation for $\xi = O(1)$ and the replacement of the decay in $\exp(-\sqrt{J}|\xi|)$ of the quasi-geostrophic solution by a decay in $\exp(-\sqrt{J}|\sin^{-1}\xi|)$. This is demonstrated explicitly by the WKB solution of Appendix A.2. Fig. 2a also compares the value of $\Psi(0)$ with its large-J (quasi-geostrophic) estimate, confirming the validity and usefulness of the estimate.

The amplitude of the non-dimensional EP-fluxes, between and beyond the inertial levels $\xi = \pm 1$, is shown in Fig. 2b. The exact results are compared with the large-J estimates which again prove accurate for J as small as 1. The figure, like Fig. 2a, illustrates the strong sensitivity of the GW generation to J.

4 Solutions for various PV-distribution

To gauge the possible importance of sheared PV anomalies as a mechanism of GW generation, we now evaluate the GW field produced by a variety of localized anomalies. From now on, we report the results in dimensional form.

We compute the perturbation fields on a grid by evaluating the integral (2.10) numerically for different initial PV distributions $q_0'(x,z)$ using the analytical solutions derived in Section 3. The computational domain $-X < x < X$ and $-Z < z < Z$ is discretised in a regular grid

with $2L+1$ points in the horizontal and $2M+1$ in the vertical. Correspondingly, the Fourier transform $\hat{q}_0(k,z)$ is also discretised and given as $\hat{q}_0(k_l,z_m)$, where $k_l = \pi l/X$, $l = -L,\cdots,L$ and $z_m = \pi m/Z$ $m = -M,\cdots,M$. In the computations presented below, we typically take $X = 4000$ km, $Z = 10$ km, $L = 2048$, and $M = 200$ which ensures excellent resolutions in both directions of propagation as well as in the spectral space.

Given $\hat{q}_0(k_l,z_m)$, the perturbation PV at different times is computed as

$$q'(x,z,t) \approx \Delta k \Delta z \sum_{-L}^{L}\sum_{-M}^{M} \hat{q}_0(k_l,z_m) e^{(ik_l x - ik_l \Lambda z_m t)} \delta\left(z - z_m\right), \tag{4.1}$$

where the values of x and z lie on the grid, $\Delta k = \pi/(LX)$ and $\Delta z = Z/M$. The perturbation streamfunction then takes the analogous form

$$\psi'(x,z,t) \approx \Delta k \Delta z \sum_{-L}^{L}\sum_{-M}^{M} \hat{\psi}_0(k_l,z_m) e^{(ik_l x - ik_l \Lambda z_m t)} \Psi\left(\frac{k_l \Lambda}{f}(z - z_m)\right), \tag{4.2}$$

where $\hat{\psi}_0(k_l,z_m) = g\rho_r \hat{q}_0(k_l,z_m)/(k\theta_r\Lambda^2)$ (see (2.10) and (2.14)). Similar expressions can be written down for u', v', w' and θ' using (2.11)–(2.12).

4.1 Monochromatic, infinitely thin PV

The simplest case that we consider is that of uniform PV, with value q_r, in a layer of depth σ_z which varies monochromatically with wavelength $2\pi/k_r$. Modelling this layer as infinitely thin corresponds to taking

$$q_0'(x,z) = \sigma_z\, q_r e^{ik_r x}\delta(z). \tag{4.3}$$

The associated streamfunction is then simply

$$\psi'(x,z) = \sigma_z \psi_r e^{ik_r x} \Psi\left(\frac{k_r\Lambda}{f} z\right), \tag{4.4}$$

where $\psi_r = g\rho_r q_r/(k_r\theta_r\Lambda^2)$. This is of course nothing other than the solution discussed in section 3 except for the dimensional factor. We focus on the dimensional aspect and examine the dimensional EP flux,

$$\overline{F}^z = -\rho_r\left(\overline{u'w'} - f\frac{\overline{v'\theta'}}{\theta_{0z}}\right) = \frac{\rho_r g^2}{f\theta_r^2 N^3}(\rho_r q_r \sigma_z)^2 \mathcal{F}^\xi\left(\frac{k_l\Lambda}{f} z\right), \tag{4.5}$$

where the overbar denotes the horizontal average.

Let us estimate an order of magnitude for this EP flux. If we consider a 1 km-thick layer of stratospheric air entering in the troposphere, we can take a PV amplitude of $\rho_r q_r = 1\,\mathrm{PVU}$, yielding $\rho_r q_r \sigma_z = 10^{-3}\,\mathrm{K\,s^{-1}}$. Assuming that this air enters the troposphere at midlatitudes, we take $\rho_r = 1\,\mathrm{kg\,m^{-3}}$, $N = 0.01\,\mathrm{s^{-1}}$, $\theta_r = 300\,\mathrm{K}$, and $f = 10^{-4}\,\mathrm{s^{-1}}$. For these parameters the dimensional factor in Eq. (4.5)

$$\rho_r \frac{g^2}{f\theta_r^2 N^3}(\rho_r q_r \sigma_z)^2 = 10\,\mathrm{Pa}. \tag{4.6}$$

Thus, the value of the non-dimensional flux $\mathcal{F}^\xi$ needs to be multiplied by 10 Pa to be dimensionally meaningful. This scaling, which is independent of the horizontal wavenumber k_r, is used in Fig. 2 for the axis on the right of the panel. For J between 1 and 10, the EP flux is seen to be between 0.1 and 100 mPa. This covers the range of values measured in the lower stratosphere away from mountains during the constant-level-balloon Vorcore campaigns (Hertzog et al. 2008).

4.2 Horizontally localized, infinitely thin PV

We now consider a PV distribution that is localized in the horizontal, but can still be modelled as infinitely thin in the vertical. Choosing a Gaussian profile in the horizontal, we represent the initial PV as

$$q_0'(x,z) \approx \sigma_z q_r e^{-x^2/(2\sigma_x^2)} \delta(z), \tag{4.7}$$

where σ_x gives the width of the PV distribution, by taking in (4.1)

$$\hat{q}_0(k_l, z_m) = \begin{cases} \dfrac{\sigma_x \sigma_z q_r}{\sqrt{2\pi}\Delta z} e^{-k_l^2 \sigma_x^2/2} & \text{for } z_m = 0 \\ 0 & \text{for } z_m \neq 0 \end{cases} .$$

The vertical velocity field corresponding to this distribution of PV is shown in Fig. 3. The width of the PV anomaly has been taken as $\sigma_x = 40$km (which corresponds to about 0.5° of longitude when $f = 10^{-4}\mathrm{s}^{-1}$); the other parameters are as in the preceding subsection. The four panels are obtained for different values of the shear Λ and hence of J, with the value of N kept constant.

For small values of J ($J = 2$ and $J = 5$), there are clear differences in the response to the PV anomaly between a region immediately surrounding the PV anomaly and the two far-field regions. The transition between these three regions can be located around the altitudes $z_I = \pm f\sigma_x/\Lambda$ of the inertial levels of disturbances with wavelength $1/\sigma_x$ (for $J = 2$ and 5, $z_I = \pm 500\,\mathrm{m}$ and $z_I = \pm 1\,\mathrm{km}$ respectively). In what follows, we term the transition regions inertial layers. Between the inertial layers, the vertical velocity is everywhere positive to the west of the positive PV disturbance (i.e. for $x > 0$) and negative to the east. This is because the transverse wind v' is cyclonic (with $v' > 0$ for $x > 0$ and $v' < 0$ for $x < 0$) and the meridional advection of background potential temperature $-f\Lambda v'$ in (2.1d), is balanced by the vertical advection $N^2 w'$. Note also that the vertical velocity is almost untilted in the vertical in this region and decreases in amplitude when $|z|$ increases. This indicates that the dynamics near $z = 0$ is well predicted by the quasi-geostrophic theory.

Above and below the inertial layers, the disturbance has a propagating character, with w' changing sign with altitude at a given horizontal location. In these two regions, w' is also tilted against the shear indicating upward propagation in the upper region and downward propagation in the lower one. The GW signal is comparable in magnitude with the signal near the PV anomaly for $J = 2$ (Fig. 3a) but substantially smaller when $J = 5$ (Fig. 3b). For even larger J (Figs. 3c and 3d) the GW signal becomes very weak, so weak as to be undetectable for $J = 25$.

As noticed, the fact that the PV disturbance is not monochromatic spreads the inertial levels over an inertial layer of finite depth. To illustrate how this affects the interactions with the large scales, Fig. 4 shows the averaged EP flux evaluated as

$$\overline{F}^z(z) = -\frac{1}{2\sigma_x} \int_{-\infty}^{+\infty} \rho_r \left(u'w' - f \frac{v'\theta'}{\theta_{0z}} \right) dx \tag{4.8}$$

from the discrete approximations to of u', w', v' and θ'. The EP flux is almost constant between the inertial layers, falls off by a factor of about two across the inertial layers, and is constant beyond. This suggests that substantial wave-mean flow interactions can occur at distances of up to a few kilometers from PV anomalies.

Note that the value of the EP flux in the far-field can be estimated analytically. Returning to the continuous formalism, using the Gaussian distribution (4.7) and the fact that $\mathcal{F}^\xi$ is

constant and independent of k for $\xi > 1$ gives.

$$\overline{F}^z \sim \sqrt{\pi}\frac{\rho_r g^2}{f\theta_r^2 N^3}(\rho_r q_r \sigma_z)^2 \mathcal{F}^\xi(\xi > 1), \quad \text{as } z \to \infty, \tag{4.9}$$

as in the monochromatic case (4.5), up to the multiplicative factor $\sqrt{\pi}$.

4.3 Horizontally localized, finite-depth PV

The PV anomalies examined in Sections 4.1 and 4.2 are approximated as infinitely thin layers. This approximation neglects the vertical shearing of the PV and hence the changes that this induces in the horizontal distribution of the PV. If this shearing occurs very rapidly, the results obtained so far are only relevant for a short time, after which the GW emission stops. To assess this, and more generally to demonstrate how our results predict a time-dependent GW generation, we now consider a PV distribution which has a finite depth. For simplicity, we take a PV distribution which is separable in x and z at $t = 0$. Specifically, we choose

$$\hat{q}_0(k_l, z_m) = \begin{cases} \dfrac{\sigma_x q_r}{\sqrt{2\pi}\Delta z} e^{-k_l^2\sigma_x^2/2}\cos^2(\pi z_m/\sigma_z) & \text{for } |z_m| < \sigma_z/2 \\ 0 & \text{for } |z_m| > \sigma_z/2 \end{cases},$$

which has the same vertical integral as (4.7).

The time-dependent streamfunction corresponding to the PV is computed according to (4.2). Because x and t enter (4.2) only in the combination $x - \Lambda z_m t$ it is possible to reduce considerably the computations involved by summing vertical and horizontal translations of the solution in Section 4.2. To illustrate briefly how the horizontal translations are done, for fixed z_m, the sum over the index l of the wavenumber k_l at some time t and for values of x on the grid can be inferred from the corresponding sum for $t = 0$ provided that t is a integer multiple of $\Delta x/(\Lambda\Delta z)$. We have adjusted our grid size to take advantage of this for the values of t chosen for the results presented.

Fig. 5 shows the evolution of the disturbance PV (grey shading) and of the vertical velocity it produces for $\sigma_z = 1\,\text{km}$, $J = 5$ and all other parameters as in the previous sections. The solution is shown only for negative values of t. Indeed, the symmetries in our problem are such that, for the shallow PV disturbances considered, the solutions for positive t are almost symmetric to that at negative t. The background velocity shears the PV which is strongly tilted against the shear for large negative time and with the shear for large positive time (not shown). Accordingly, the width of PV distribution is deeply altered, decreasing here by a factor of almost 2 from $t = -24$ h to $t = 0$. As a result, the vertical-velocity signal has a decreasing width and increasing amplitude as t increases towards 0.

Comparing the four panels in Fig. 5 to the (time-independent) disturbance produced by the infinitely thin distribution of Fig. 3b indicates that the GW patterns in the far field are comparable at $t = -1\,2$h and almost identical at $t = 0\,$h. Accordingly, and because the EP flux is a quadratic quantity, it is only in a time interval of a day or so that we can expect the EP flux to approach the values shown in Fig. 4. This last point is confirmed by Fig. 6 which displays the evolution of $\overline{F}^z$ evaluated at $z = -10$ km for the finite-depth PV anomaly. For all values of J, the EP flux peaks at $t = 0$, with peak values that compare well with the (time-independent) values obtained for the infinitely thin distribution (see Fig. 4 and (4.9)). The peak in EP flux shown in Fig. 6 broadens as J increases because the PV advection also slows down. Nevertheless the characteristic durations of the burst in EP flux remains of the order of a day in the range of J considered here.

Although this last result is quite sensitive to the spatial extent of the PV distribution (with the characteristic duration of the EP flux bursts decreasing when the depth of the PV disturbance increases and/or when its width decreases) it clearly illustrates that our mechanism of GWs generation is quite robust: the EP flux in the far field predicted by (4.9) at some time are representative of the flux within a few hours of that time. This is important for the parameterization of the GWs produced by PV anomalies in GCMs, since these parameterization schemes can realistically be updated every few hours.

5 Summary and applications

5.1 Summary

In the presence of a uniform vertical shear, and in the absence of boundaries in the vertical, localised PV anomalies produce disturbances to which are associated two inertial layers. These layers are located above and below the PV anomaly, at a distance $z_I = \sigma_x f/\Lambda$, where σ_x is the typical width of the PV anomaly. Between these two inertial layers, the form of the disturbance is qualitatively well predicted by the quasi-geostrophic theory, and geostrophic balance is a good approximation for the meridional wind in this region. Accordingly, the decay with altitude of the disturbance amplitude is exponential with a decay rate of the order of $\frac{N}{f\sigma_x}$. Beyond the inertial layers, the intrinsic frequency of the disturbance is larger than f so the disturbance propagates vertically in the form of a GW. If the disturbance amplitude is substantial at the inertial level, the GW amplitudes produced by this mechanism can be significant. This condition is satisfied provided $\frac{z_I N}{f\sigma_x} = N/\Lambda = \sqrt{J}$ is not large. More specifically, we show that the amplitude of the GW is near $\exp(-\sqrt{J}\pi/2)/(2J)$ for $J > 1$. Correspondingly, the Eliassen–Palm flux associated with the GW depends also exponentially on J, scaling almost like $\exp(-\pi\sqrt{J})/8$ beyond the inertial levels, and almost like $\exp(-\pi\sqrt{J})/4$ between them.

The robustness of these results has been tested numerically, and for the case of a PV disturbance localized horizontally and of finite depth. Horizontal localization spreads the inertial level of the monochromatic case over an inertial layer, and finite depth leads to a time-dependent perturbation. It is nevertheless shown that under these circumstances the GW amplitudes and the EP fluxes in the far field remain well predicted by the monochromatic results, with multiplicative factors that are of order one (see (4.9)). The characteristic time over which they evolve is also found to exceed a few hours, suggesting that our formula can usefully predict the EP fluxes produced by PV anomalies, for instance if these anomalies are diagnosed every hour.

5.2 Applications

These results can be directly useful for the parameterization of GWs in GCMs that include the middle atmosphere. The dimensional results of section 4 suggest that the EP fluxes in the far-field produced by localized PV anomalies compare in amplitude with the EP fluxes measured in the low stratosphere by constant level balloons during the Vorcore campaign. Although the analytical expressions we give are well suited to this context, notably because the GW-parameterization routines typically re-evaluate the EP fluxes according to the large-scale flow every hour, they require an estimation of the PV anomalies at subgrid scales.

In most of the parameterizations used currently, the GW EP fluxes from the troposphere toward the middle atmosphere are imposed regardless of the GWs tropospheric sources. There are nevertheless some exceptions, like in Charron and Manzini (2002), where the GW amplitude

is larger if fronts are identified. Our formula in (3.20) could well be used in this context since large PV anomalies form during frontogenesis. It could therefore be used to parametrize quantitatively the GW radiated by fronts as well as and by other processes that induce localized PV anomalies.

Our results are also relevant to the problem of non-modal growth of baroclinic disturbances (Farrel 1989). In fact, the inertial levels, which are ignored in balanced approximations, change the boundary conditions at large distances from the critical level from decay conditions into radiation conditions; as a result the global structure of the solutions in the continuous spectrum is deeply altered. As a result, an inflow PV anomaly of short horizontal-scales can have a much larger surface signature than predicted by balanced models. This is because the disturbances produced in this case can have an inertial layer between the PV and the surface. As our solutions are the non-geostrophic counterpart of the building blocks that are used by Bishop and Heifetz (2000) to explain the triggering of storms by upstream PV anomalies, or to explain the optimal perturbations evolution by DeVries and Opsteegh (2007), they may be useful to examine these problems in the non-geostrophic case.

Finally, our results could be useful to study the evolution of initial disturbances, or of disturbances produced by any external causes (the classical adjustment problem). For this purpose, it should nevertheless be noticed that the modes with Dirac PV are not the only modes associated with the continuous spectrum. In fact, for each value of the phase velocity, there are two further singular modes, with zero PV and singular behaviour of the other fields at the inertial levels. These modes are essential to the completeness of the modal representation of the solutions.

Acknowledgments. This work was supported by the Alliance programme of the French Foreign Affairs Ministry and British Council. J.V. acknowledges the support of a NERC grant.

A Approximate solutions

A.1 Quasi-geostrophic approximation

The quasi-geostrophic approximation can be recovered by approximating the perturbation PV as

$$\rho_r q_g' = \overline{\theta}_{0z} \partial_x v' + f \partial_z \theta'. \tag{A.1}$$

Using the polarisation relations (2.11-2.12), the QG-PV equation has a streamfunction solution ψ_g' that can be written as a spectral expansion similar to (2.10), where $\hat{\psi}_0$ is as in (2.14) and $\Psi(\xi)$ is replaced by the structure function $\Psi_g(\xi)$. This new structure function $\Psi_g(\xi)$ is solution of the QG approximation of the structure (2.15), namely

$$\left(\frac{1}{\xi^2}\right) \Psi_{g\xi\xi} - \frac{2}{\xi^3} \Psi_{g\xi} - \frac{J}{\xi^2} \Psi_g = \delta(\xi). \tag{A.2}$$

The solution vanishing for $|\xi| \to \infty$ is given by

$$\Psi_g = \frac{|\xi|}{2J} e^{-\sqrt{J}|\xi|} + \frac{1}{2\sqrt{J^3}} e^{-\sqrt{J}|\xi|}. \tag{A.3}$$

A.2 WKB approximation

In this section, we solve the differential equation (2.15) asymptotically using a WKB method. This method has the interest of providing the solution in terms of (mostly) elementary functions: these reveal the structure of the solution more explicitly than the exact solutions do.

To derive an approximate homogeneous solution $\Psi^{(u)}(\xi)$ valid for $\xi > 0$, we distinguish four different regions in which $\Psi^{(u)}(\xi)$ takes a different asymptotic form: (i) an inner region with $\xi \ll 1$; (ii) an outer region with $O(1) = \xi < 1$; (iii) an inner region for $\xi \approx 1$; and (iv) a second outer region for $\xi > 1$. In the outer regions (ii) and (iv), two independent solutions are found by introducing the WKB ansatz

$$\Psi^{(u)} = (f_0 + J^{-1/2} f_1 + \cdots) e^{\sqrt{J}\int^{\xi} \phi(\xi')\, d\xi'}$$

to find that

$$\phi = \frac{\pm 1}{\sqrt{1-\xi^2}} \quad \text{and} \quad f_0 = \frac{A\xi}{\sqrt{\phi}\sqrt{\xi^2-1}} = \frac{A\xi}{(1-\xi^2)^{1/4}},$$

for some constant A. Thus we obtain

$$\Psi^{(u)} \sim \frac{\xi}{(1-\xi^2)^{1/4}} \left(A^{(\mathrm{ii})} e^{-\sqrt{J}\sin^{-1}\xi} + B^{(\mathrm{ii})} e^{\sqrt{J}\sin^{-1}\xi} \right) \tag{A.4}$$

in region (ii), and

$$\Psi^{(\mathrm{u})} \sim \frac{\xi}{(\xi^2-1)^{1/4}} \left(A^{(\mathrm{iv})} e^{i\sqrt{J}\ln(\xi+\sqrt{\xi^2-1})} + B^{(\mathrm{iv})} e^{-i\sqrt{J}\ln(\xi+\sqrt{\xi^2-1})} \right) \tag{A.5}$$

in region (iv), where $A^{(\mathrm{ii})}$, $B^{(\mathrm{ii})}$, $A^{(\mathrm{vi})}$ and $B^{(\mathrm{vi})}$ are arbitrary constants. The proper radiation condition as $\xi \to \infty$ is satisfied by (A.5) provided that

$$B^{(\mathrm{vi})} = 0.$$

The WKB solutions (A.4)–(A.5) break down as the inner regions are approached and (2.15) needs to be rescaled. For region (i), we introduce $Z = \sqrt{J}z$ into (2.15) and obtain at leading order the equation

$$\Psi_{ZZ} - \frac{2}{Z}\Psi_Z - \Psi_Z = 0,$$

which is equivalent to the quasi-geostrophic approximation (A.2) and giving

$$\Psi^{(u)} \sim A^{(\mathrm{i})} e^{-\sqrt{J}\xi}(\sqrt{J}\xi + 1) + B^{(\mathrm{i})} e^{\sqrt{J}\xi}(\sqrt{J}\xi - 1). \tag{A.6}$$

In region (iv), we introduce the scaled variable $\zeta = J(\xi - 1)$ and obtain the leading-order equation

$$2\zeta\Psi_{\zeta\zeta} + 2\Psi_\zeta + \Psi = 0.$$

The solution can be conveniently written in terms of Hankel functions (AS, Ch. 9)

$$\Psi^{(u)} \sim A^{(\mathrm{iii})} H_0^{(1)}(\sqrt{2J(\xi-1)}) + B^{(\mathrm{iii})} H_0^{(2)}(\sqrt{2J(\xi-1)}). \tag{A.7}$$

The response to a Dirac of PV can then be constructed as in (3.11) by combining $\Psi^{(u)}(\xi)$ for $\xi > 0$ with $[\Psi^{(u)}(-\xi)]^*$ for $\xi < 0$. The jump condition at $\xi = 0$, applied to (A.6) gives

$$A^{(\mathrm{i})} + B^{(\mathrm{i})} = \frac{1}{2J^{3/2}}. \tag{A.8}$$

All the constants can then be obtained by matching the various asymptotic results across regions. Matching between regions (i) and (ii) gives

$$\sqrt{J}A^{(\mathrm{i})} = A^{(\mathrm{ii})} \quad \text{and} \quad \sqrt{J}B^{(\mathrm{i})} = B^{(\mathrm{ii})}.$$

To match between (ii) and (iii), we recall the branch choice (3.8) and note the asymptotic formulas

$$H_0^{(1)}(x) \sim \sqrt{\frac{2}{\pi x}} e^{i(x-\pi/4)} \quad \text{and} \quad H_0^{(2)}(x) \sim \sqrt{\frac{2}{\pi x}} e^{-i(x-\pi/4)}, \tag{A.9}$$

valid for $|x| \to \infty$, and $-\pi < \arg x < 2\pi$ and $-2\pi < \arg x < \pi$, respectively (9.2.3–4 in AS). Using this in (A.7) and comparing with the expansion of (A.4) for $\xi \to 1^-$ gives

$$e^{-\sqrt{J}\pi/2} A^{(\mathrm{ii})} = \frac{2^{1/2}}{\pi^{1/2} J^{1/4}} A^{(\mathrm{iii})} \quad \text{and} \quad e^{\sqrt{J}\pi/2} B^{(\mathrm{ii})} = i \frac{2^{1/2}}{\pi^{1/2} J^{1/4}} B^{(\mathrm{iii})}.$$

Similarly, comparing with the expansion of (A.5) for $\xi \to 1^+$ gives

$$A^{(\mathrm{iv})} = \frac{2^{1/2} e^{-i\pi/4}}{\pi^{1/2} J^{1/4}} A^{(\mathrm{iii})} \quad \text{and} \quad B^{(\mathrm{iv})} = \frac{2^{1/2} e^{i\pi/4}}{\pi^{1/2} J^{1/4}} B^{(\mathrm{iii})}.$$

Since the radiation condition for large ξ implies that $B^{(\mathrm{iv})} = 0$, we conclude that

$$B^{(\mathrm{i})} = B^{(\mathrm{ii})} = B^{(\mathrm{iv})} = 0.$$

It follows that $A^{(\mathrm{i})} = 1/(2J^{3/2})$ and hence that

$$A^{(\mathrm{i})} = \frac{1}{\sqrt{J}} A^{(\mathrm{ii})} = \frac{e^{i\pi/4} e^{\sqrt{J}\pi/2}}{\sqrt{J}} A^{(\mathrm{iv})} = \frac{1}{2J^{3/2}}.$$

Thus we find that $\Psi(0) \sim 1/(2J^{3/2})$ and that the gravity-wave amplitude is $|A^{(\mathrm{iv})}| \sim e^{-\sqrt{J}\pi/2}/(2J)$, consistent with (3.15) and (3.18), respectively. The EP flux $\mathcal{F}^{\xi} \sim e^{-\sqrt{J}\pi}/8$ for $|\xi| > 1$ follows immediately, consistent with (3.20). The evaluation of the EP flux for $|\xi| < 1$ is more delicate because it includes terms that are exponentially small in $\sqrt{J}$ and are ignored here.

References

Abramowitz M. and I. A. Stegun, 1964: Handbook of mathematical functions (9th edition), *Dover Publications, Inc., New York*, pp. 1045.

Bakas, N. A. and P. J. Ioannou, 2007: Momentum and energy transport by gravity waves in stochastically driven stratified flows. Part I: Radiation of gravity waves from a shear layer, *J. Atmos. Sci.,***64,** 1509-1529.

Blumen, W., 1972: Geostrophic adjustment, *J. Atmos. Sci.,***10,** 485–528.

Bishop, C.H. and E. Heifetz, 2000: Apparent absolute instability and the continuous spectrum, *J. Atmos. Sci.,***57,** 3592–3608.

Booker, J.R. and F.P. Bretherton, 1967: The critical layer for internal gravity waves in a shear flow, *J. Fluid Mech.*, **27**, 513–539.

Bretherton, C.S., and P.K. Smolarkiewicz, 1989: Gravity-waves, compensating subsidence and detrainment around cumulus clouds, *J. Atmos. Sci.,***46,** 740–759.

Charron, M. and E. Manzini, 2002: Gravity waves from fronts: Parameterization and middle atmosphere response in a general circulation model, *J. Atmos. Sci.,***59,** 923–941.

DeVries H. and H. Opsteegh, 2007: Resonance in optimal perturbation evolution. Part I: Two-layer Eady model, *J. Atmos. Sci.,***64,** 673–674.

Eliassen, A. and E. Palm, 1961: On the transfer of energy in stationary mountain waves, *Geophys. Publ.,***22,** 1–23.

Farrel, B. F., 1989: Optimal excitation of baroclinic waves, *J. Atmos. Sci.,***46,** 1193-1206.

Ford, R., M.E. McIntyre, and W.A. Norton, 2000: Balance and the slow quasimanifold: Some explicit results, *J. Atmos. Sci.,***57,** 1236–1254.

Fritts, D. C., and Z. Luo, 1992: Gravity wave excitation by geostrophic adjustment of the jet stream, *J. Atmos. Sci.* **, 49,** 681–697.

Hertzog, A, G. Boccara, R. A. Vincent, F. Vial, and P. Cocquerez, 2008: Estimation of gravity wave momentum flux and phase speeds from quasi-Lagrangian stratospheric balloon flights. Part II: Results from the Vorcore campaign in Antarctica, *J. Atmos. Sci.,* **65,** 3056–3070.

Inverarity, G.W. and G.J. Shutts, 2000: A general, linearized vertical structure equation for the vertical velocity: Properties, scalings and special cases, *Quart. J. Roy. Meteor. Soc.,*,**126**, 2709–2724.

Jones, W.L., 1967: Propagation of internal gravity waves in fluids with shear flow and rotation, *J. Fluids Mech.***, 30,** 439-448.

Lalas, D.P. and F. Einaudi, 1976: Characteristics of gravity-waves generated by atmospheric shear layers, *J. Atmos. Sci.,* **33,** 1248–1259.

Lott, F., H. Kelder, and H. Teitelbaum, 1992: A transition from Kelvin-Helmholtz instabilities to propagating wave instabilities, *Phys. Fluids,***4,** 1990-1997.

Lott, F., 1997: The transient emission of propagating gravity waves by a stably stratified shear layer, *Quart. J. Roy. Meteor. Soc.,* **123**, 1603–1619.

Lott, F., 2003: Large-scale flow response to short gravity waves breaking in a rotating shear flow, *J. Atmos. Sci.,* **60,** 1691–1704.

Molemaker, M.J., J.C. McWilliams and I. Yavneh, 2005: Baroclinic instability and loss of balance, *J. Phys. Oceano.,***35,** 1505–1517.

Olafsdottir, E. I., A. B. O. Daalhuis and J. Vanneste, 2008: Inertia-gravity-wave radiation by a sheared vortex, *J. Fluid Mechanics,* **596,** 169–189.

Pedlosky, J., 1979: Geophysical fluid dynamics, *Springer - Verlag*, pp. 180.

Plougonven, R., D.J. Muraki and C Snyder, 2005: A baroclinic instability that couples balanced motions and gravity waves, *J. Atmos. Sci.,* **62,** 1545–1559.

Rosenthal, A.J. and R.S. Lindzen, 1983: Instabilities in a stratified fluid having one critical-level 1: Results, *J. Atmos. Sci.,* **40**, 509–520.

Rossby, C. G., 1937: On the mutual adjustment of pressure and velocity distributions in certain simple current systems, *J. Mar. Res.* **, 21,** 15-28.

Scavuzzo, C.M., Lamfri, M.A., Teitelbaum, H. and F. Lott, 1998: A study of the low frequency inertio-gravity waves observed during PYREX, *J. Geophys. Res.*, *D2*, *103*, 1747–1758.

Shutts, G.J., and M.E.B. Gray, 1994: A numerical modeling study of the geostrophic adjustment process following deep convection, *Quart. J. Roy. Meteor. Soc.,* **120,** 1145–1178.

Vanneste J. and I. Yavneh, 2004: Exponentially small inertia-gravity waves and the breakdown of quasigeostrophic balance *J. Atmos. Sci.,* **61,** 211–223.

Vanneste J., 2008: Exponential smallness of inertia-gravity-wave generation at small Rossby number, *J. Atmos. Sci.*, **65,** 1622-1637.

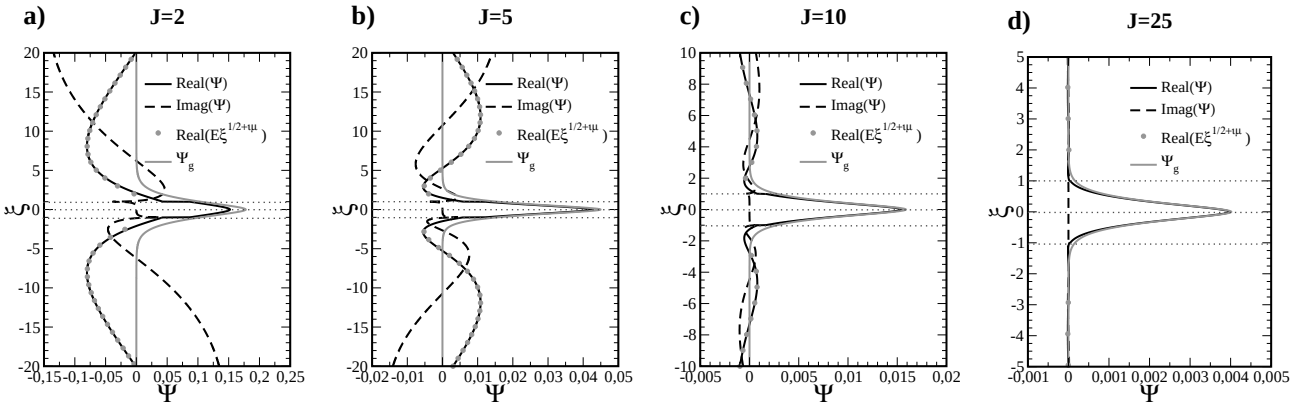

Figure 1: Structure function $\Psi(\xi)$ associated with a monochromatic PV distribution proportional to $\delta(\xi)$ for a Richardson number $J = 2$ (a), 5 (b), 10 (c) and 25 (d). The thick black curves and thick dotted curves show the real and imaginary parts of Ψ, respectively, the thick grey cuves show the quasi-geostrophic approximation Ψ_g, and the grey dots show the real part of the far-field, gravity-wave approximation $E\xi^{1/2+i\mu}$.

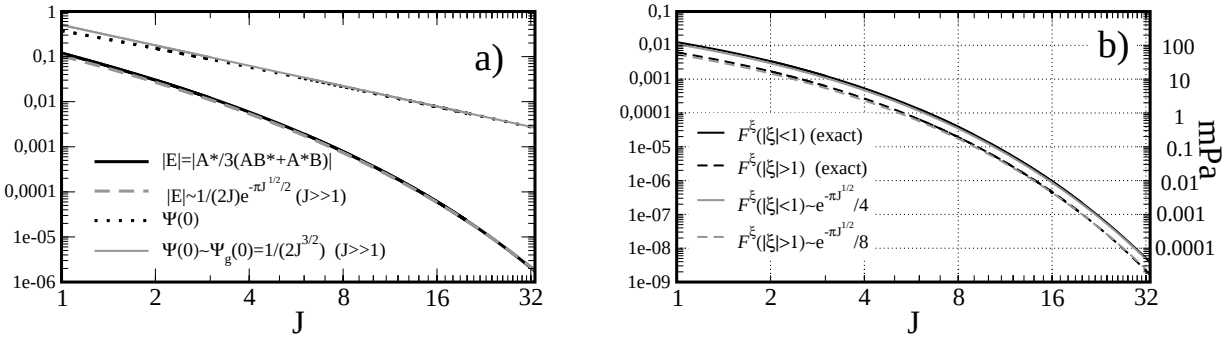

Figure 2: Characteristic amplitudes of the disturbances produced by the dirac PV anomaly: Panel (a) Exact and approximate values for the GW amplitude $|E|$ given by (3.18) (black solid curve and grey dashed curve, respectively); exact and approximate values of $\Psi(0)$ given by (3.15) (grey solid curve and black dots, respectively); Panel (b) Exact and approximate values of the EP flux F^{ξ} between the inertial levels (black solid curve and grey solid curve); exact and approximate values of F^{ξ} beyond the inertial levels (black dashed curve and grey dashed curve) see (3.20). The axis on the right of (b) give the results in the dimensional form corresponding to the parameter choice (4.6).

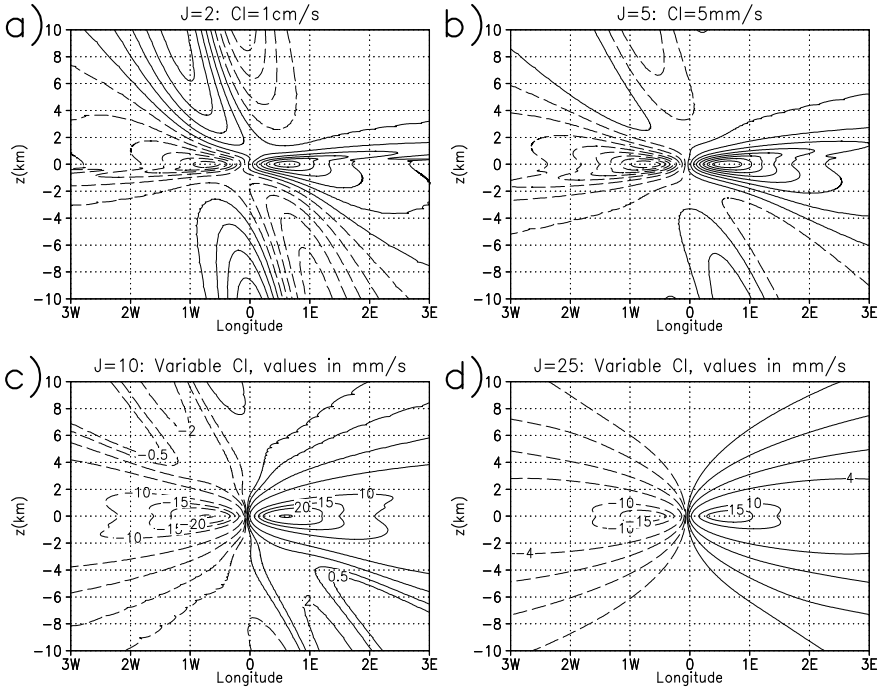

Figure 3: Vertical velocity induced by an horizontally localised but infinitely thin PV anomaly (see the PV horizontal profile in (4.7)) for $J = 2$ (a), 5 (b), 10 (c) and 25 (d), with dashed curves indicating negative values. The contour interval, indicated on each panel, varies from one panel to the other.

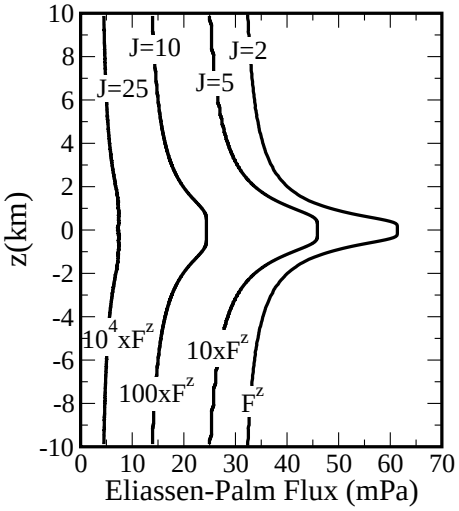

Figure 4: Vertical profiles of Eliassen–Palm flux for the four solutions in Fig 3. Note the rescaling of the flux for the different values of J.

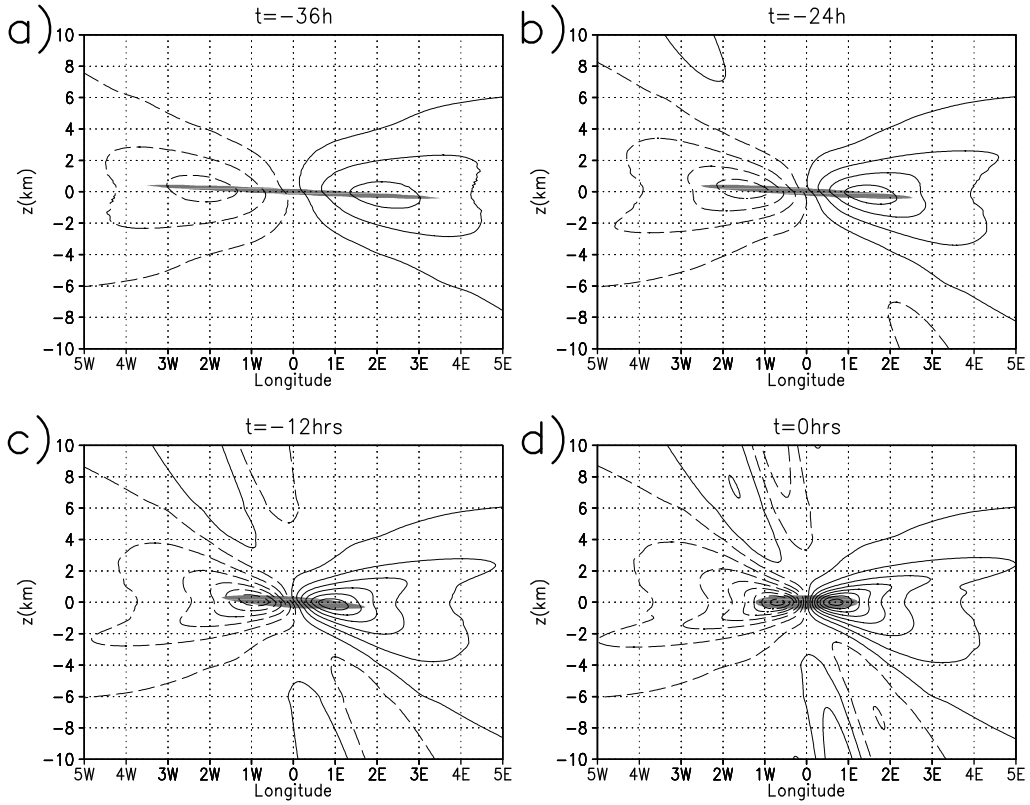

Figure 5: Evolution of the vertical velocity field associated with the evolution of a PV disturbance of finite depth, finite width and a maximum value of 1 PVU. The PV-values above 0.1 PVU are shaded, and the contours for the vertical velocity are as in Fig. (3)b

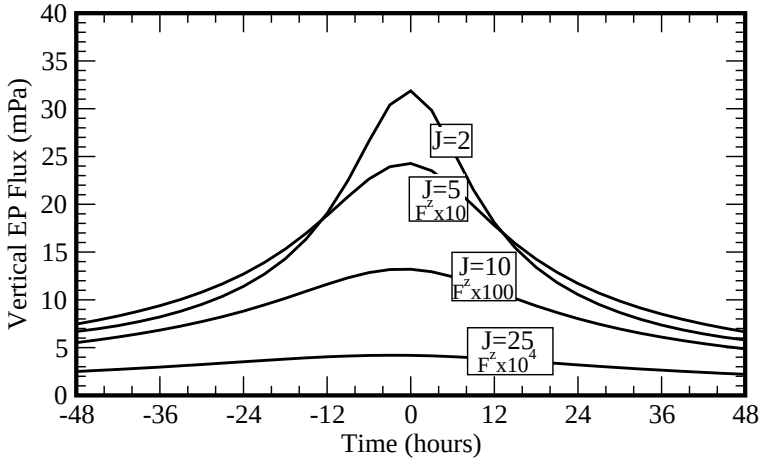

Figure 6: Temporal evolution of the far field EP flux for finite-depth, finite-width PV anomaly and for different values of the Richardson number J. Note that the EP flux has been rescaled as in Fig. 4.